Heliyon 10 (2024) e36275

Contents lists available at ScienceDirect

Heliyon

journal homepage: www.cell.com/heliyon

Research article

Increased DNA damage of adipose tissue-derived mesenchymal stem cells under inflammatory conditions

Zoltán G. Páhi [a,b], Diána Szűcs [c,d,e], Vanda Miklós [a,f], Nóra Ördög [b,c,d], Tamás Monostori [c,e], János Varga [e], Lajos Kemény [c,e,g], Zoltán Veréb [c,e,**,1], Tibor Pankotai [a,b,*]

[a] Hungarian Centre of Excellence for Molecular Medicine (HCEMM), Genome Integrity and DNA Repair Core Group, University of Szeged, Szeged, Hungary
[b] Department of Pathology, Albert Szent-Györgyi Medical School, University of Szeged, Szeged, Hungary
[c] Competence Centre of the Life Sciences Cluster of the Centre of Excellence for Interdisciplinary Research, Development and Innovation, University of Szeged, Szeged, Hungary
[d] Doctoral School of Clinical Medicine, University of Szeged, Szeged, Hungary
[e] Regenerative Medicine and Cellular Pharmacology Laboratory, Department of Dermatology and Allergology, University of Szeged, Szeged, Hungary
[f] USZ Biobank, University of Szeged, Szeged, Hungary
[g] Hungarian Centre of Excellence for Molecular Medicine (HCEMM), HCEMM-USZ Skin Research Group, University of Szeged, Szeged, Hungary

ARTICLE INFO

Keywords:
DNA repair
ADMSC
RNAseq
Stem cells
NHEJ

ABSTRACT

Cells have evolved various DNA repair mechanisms to prevent DNA damage from building up. Malfunctions during DNA repair can influence cellular homeostasis because they can bring on genomic instability through the improper recognition of DNA damage or dysregulation of the repair process. Maintaining proper DNA repair is also essential for stem cells (SCs), as they provide a differentiated cell population to the living organism. SCs are regularly used in personalized stem cell therapy. Patients must be treated with specific activators to produce these SCs effectively. This report investigated the impact of treating mesenchymal stem cells (MSC) with lipopolysaccharide, tumor necrosis factor, interferon-gamma, polyinosinic acid, interleukin 1 beta, while monitoring their transcription-related response using next-generation sequencing. RNA sequencing revealed robust gene expression changes, including those of specific genes encoding proteins implicated in DNA damage response. Stem cells can effectively repair specific DNA damages; moreover, they fail to undergo senescence or cell death when genetic lesions accumulate. Here, we draw attention to an elevated DNA repair activation following MSC induction, which may be the main reason for the ineffective stem cell transplantation and may also contribute to the genetic drift that can initiate tumor formation.

* Corresponding author. Hungarian Centre of Excellence for Molecular Medicine (HCEMM), Genome Integrity and DNA Repair Core Group, University of Szeged, Szeged, Hungary.
** Corresponding author. Competence Centre of the Life Sciences Cluster of the Centre of Excellence for Interdisciplinary Research, Development and Innovation, University of Szeged, Szeged, Hungary.
E-mail addresses: vereb.zoltan@med.u-szeged.hu (Z. Veréb), pankotai.tibor@szte.hu (T. Pankotai).
[1] Lead author: vereb.zoltan@med.u-szeged.hu

https://doi.org/10.1016/j.heliyon.2024.e36275
Received 8 March 2024; Received in revised form 7 August 2024; Accepted 13 August 2024
Available online 20 August 2024

1. Background

Due to their self-renewal capacity, stem cells can generate various differentiated cell populations, allowing tissue regeneration [1]. Stem cells present in adult tissues provide unlimited lineage-specific differentiation during embryonic developmental stages. Some of these cells can divide without differentiation, while the differentiated daughter cells can also aid in the reproduction of the tissue mass [2]. Mesenchymal stem cells (MSCs) are immature cells in nearly all adult tissues and solid organs, including the bone marrow [3]. This fact makes it possible to collect human MSCs from vascularized tissues. MSCs can initiate tissue regeneration by releasing certain factors that stimulate neighboring cells to proliferate and effectively repair damaged tissues [4]. Human MSCs have endless capacity for self-renewal, facilitating their intense therapeutic use. MSCs exhibit a unique possibility for trans-differentiation into ectodermal, neuroectodermal, or endodermal cells, called "stem cell plasticity." Moreover, MSCs possess immunosuppressive properties, suggesting their potential clinical applications in regenerative medicine and therapies for treatment-resistant immune disorders.

Since the stromal vascular fraction of human MSCs can be extracted from fat tissues (referred to as adipose-derived mesenchymal stem cells, ADMSC), and used to substitute MSCs, adipose tissue can also be considered a potential source of stem cells [5]. Therefore, adipose tissue is a valuable source of MSCs. Finally, it has been demonstrated that the site of tissue harvesting influences the MSCs' ability to regenerate mainly through their yield, proliferation, and differentiation [6]. In order to ensure the purity and quality of MSCs for clinical applications, it is crucial to monitor the processes to expand them in a robust and reproducible way.

Various DNA-damaging agents are constantly posing a threat to our genome. These assaults can derive from exogenous sources, such as UV light or ionizing radiation, and endogenous sources, such as metabolic by-products brought on by oxidative stress or replication errors. These effects may comprise one or both DNA strands. Persistent generation of errors frequently leads to translocations and genomic instability, which may cause tumorigenesis [7]. Throughout evolution, various repair mechanisms have arisen to preserve genomic integrity. DNA damage response (DDR) activates checkpoint kinases during DNA repair, which delays the cell cycle necessary for repair. DDR is initiated by the recruitment and extensive spreading of key players around the lesions, forming a repair focus [8]. The ATM (Ataxia Telangiectasia Mutated) kinase is essential to this early signaling cascade because it phosphorylates the histone variant H2AX at Ser-139 (referred to as γH2AX) which is among the first post-translational modification that appear around the lesion [9]. Regulatory mechanisms protect genomic integrity and tissue homeostasis in adult stem and progenitor cells in various tissues [10]. Dysregulation of DNA repair pathways in MSCs can restrict MSCs' ability to self-renew and differentiate, which can diminish their tissue regeneration capability [11].

This study addresses the transcriptional reprogramming of MSCs obtained from human adipose tissue following *in vitro* administration of lipopolysaccharide (LPS), tumor necrosis factor (TNF-α), interferon-gamma (IFN-γ), polyinosinic acid (PolyI:C), and interleukin 1 beta (IL-1β). After following the activation treatment, mRNA isolation and next-generation sequencing (NGS) were carried out. DNA repair-related processes were downregulated in several of the most severely impacted pathways. According to statistical analysis, the most dramatically affected processes are in association with DNA Double-Strand Break Repair. Furthermore, we observed that these expressional changes were caused by elevated DNA damage in MSCs, as indicated by increased γH2AX and 53BP1 foci in the PolyI:C-, TNF-α-, and IL1b-treated cells compared to the control, which might be the consequence of the treatment effectiveness.

2. Experimental procedures

2.1. Isolation of ADMSC

The collection of adipose tissue was in accordance with the guidelines of the Declaration of Helsinki and was approved by the National Public Health and Medical Officer Service (NPHMOS) and the National Medical Research Council (16821-6/2017/EÜIG, STEM-01/2017), which follows the Directive 2004/23/CE of the EU Member States on the practice of presumed written consent for tissue collection. Abdominal adipose tissues were removed from the patients (Sex:1/2 F/M, Age: 50.3 ± 14.5 years), and the isolation was performed within 1 h after plastic surgery, as previously described [12]. For maintaining the cell cultures, DMEM-HG medium (Biosera, Nuaille, France), supplemented with 10 % FBS (Biosera, Nuaille, France) and 1 % antibiotic–antimycotic solution was applied [13].

2.2. Characterization of ADMSC

According to the International Society for Cell and Gene Therapy (ISCT) criteria, the phenotype and differentiation capacity of ADMSCs were tested before the experiments [13,14]. Briefly, cell surface molecules were measured by flow cytometry, and the canonical three-way (adipocytes, chondrocytes, and osteocytes) *in vitro* differentiation was performed with a differentiation medium (Gibco's StemPro® Adipogenesis, Osteogenesis, and Chondrogenesis Differentiation Kits, Gibco) for 21 days. Differentiation was proved by histochemical stainings as previously published [12,13,15,16]. The surface antigen expression pattern was characterized by three-color flow cytometry using fluorochrome-conjugated antibodies with isotype-matching controls. For the measurement of the fluorochrome signal, the BD FACSAriaTM Fusion II flow cytometer (BD Biosciences Immunocytometry Systems, Franklin Lakes, NJ, USA) was applied, and data were processed by Flowing Software (Cell Imaging Core, Turku Centre for Biotechnology, Finland). The differentiation potential of adipose-tissue-derived mesenchymal stem cells was verified by differentiating into adipocyte, chondrocyte, and osteocyte lines. They were cultured in a 24-well plate, in 5×10^4 cells/well; after 24 h of incubation, the differentiation medium was added. The commercially available Gibco's StemPro® Adipogenesis, Osteogenesis, and Chondrogenesis Differentiation Kits were applied according to the manufacturer's guidelines (Gibco, Thermo Fisher Scientific, Waltham, MA USA). After 21 days of

maintenance, the cells were fixed with 4 % methanol-free formaldehyde (Molar Chemicals, Hungary) for 20 min at room temparture (RT). Differentiation stages of AD-MSCs were validated using different staining. For visualization of lipid-laden particles, Nile red staining (Sigma-Aldrich, Merck KGaA, Darmstadt, Germany) was utilized, and Alizarin red staining (Sigma-Aldrich, Merck KGaA, Darmstadt, Germany) was applied to show the mineral deposits during osteogenesis. Toluidine blue staining (Sigma-Aldrich, Merck KGaA, Darmstadt, Germany) was wielded to label the chondrogenic mass.

The data obtained from the ADMSCs characterization and the patient characteristics that have been used in this study are shown in Fig. S1.

2.3. Treatment of ADMSC by TLR ligands and pro-inflammatory factors

Cells were cultured in DMEM-HG medium (Biosera, Nuaille, France), supplemented with 10 % FBS (Biosera, Nuaille, France), 1 % L-glutamine (Biosera, Nuaille, France) and 1 % Antibiotic–Antimycotic Solution (Biosera, Nuaille, France). The cells were then subjected to various treatments: (A) LPS [100 ng/mL, tlrl-peklps, ultrapure, Invivogen, San Diego, CA, USA], (B) TNFα [100 ng/mL, 300-01A, Peprotech, London, UK], (C) IL-1β [10 ng/mL, 200-01B, Peprotech, London, UK], (D) IFNy [10 ng/mL, 300-02, Peprotech, London, UK], or (E) PolyI:C [25 μg/mL, tlrl-pic, Invivogen, San Diego, CA, USA]. After adding inflammatory agents, the cells were maintained for another 24 h under standard conditions (37 °C, in 5 % CO_2), with untreated cells as controls [12,13,15,16]. After the 24-h treatment period, the cells were harvested and processed for RNA isolation.

For RNA-seq, after trypsinizing and counting ADMSCs using an EVE automatic cell counter from NanoEntek (NanoEntek, Seoul, Korea), 3×10^5 cells were seeded in a T25 cm^2 flask in culture media described above, and the cells were grown for 24 h. After replacing the media, the following treatments were applied: (I) 100 ng/mL human recombinant TNF-α (Peprotech, London, UK), (II) 100 ng/mL LPS, (III, ultrapure, Invivogen, San Diego, CA, USA) 10 ng/mL human recombinant IL-1β (Peprotech, London, UK), (IV) 25 ng/mL PolyI:C (Invivogen, San Diego, CA, USA), (V) 10 ng/mL human recombinant IFN-γ (Peprotech, London, UK) and (VI) untreated control. Upon treatment, cells were incubated for 24 h under standard conditions (37 °C, in 5 % CO_2), and then pelleted and used for RNA isolation. Following a 24-h treatment period, cells were seeded for immunostaining. After gently washing the cells with Ca^{2+}- and Mg^{2+}-free phosphate buffered saline (PBS), they were fixed with 4 % methanol-free formaldehyde (Molar Chemicals, Hungary) for 20 min at RT.

2.4. RNA isolation

For RNA isolation, the cells were trypsinized and collected, and then the cell pellet was suspended in 1 mL TRI Reagent® (Genbiotech Argentina, Bueno Aries, Argentina) and stored at −80 °C for 24 h. After the samples had been thawed, 200 μL chloroform was added, and they were thoroughly mixed before being incubated at RT for 10 min. The samples were centrifuged at 13,400 g for 20 min at 4 °C for phase separation. After transferring the aqueous phase into new tubes, 500 μL 2–propanol was added and thoroughly mixed. Then, the incubation and phase-separation steps were repeated. Next, the pellets were washed with 750 μL 75 % EtOH–DEPC after the supernatants were removed. The samples were centrifuged at 7500 g for 5 min at 4 °C after the supernatants were decanted, and the samples were dried for 20 min at 45 °C. The pellets were suspended in RNase-free water and incubated for 10 min at 55 °C. The concentration was measured using an IMPLEN N50 UV/Vis Nanophotometer (Implen GmbH, Munich, Germany), and samples were stored at −80 °C.

2.5. NGS analysis

After single-end sequencing of each sample, FastQC was performed to check the quality of RNA sequences. We utilized the Trimmomatic tool to remove adapter sequences and filter out low-quality reads from our dataset. The parameters were set to trim reads using a sliding window approach with a window size of 4 bases and a quality threshold of 20 (SLIDINGWINDOW:4:20). Additionally, we discarded any reads shorter than 20 bases after trimming by setting the MINLEN parameter to 20. In our study, we employed the HISAT2 aligner to map RNA-seq reads against the GRCh38 reference genome, ensuring accurate alignment. Post-alignment quality control was conducted using CollectRNAseqMetrics from the Picard tools suite, which facilitated the evaluation of exon-specific alignment rates and the detection of any potential 5′-3′ transcriptional bias. For gene expression quantification, the featureCounts utility was utilized to assign reads to genomic features. Differential gene expression analysis was performed using the DESeq2 package, designed for the statistical analysis of count data and capable of handling biological variability within replicates.

In our analysis, we used the general workflow recommended by the DESeq2 package. The analysis workflow was structured as follows:

Data Preparation: We defined experimental conditions using a factor with levels corresponding to each treatment group (CTRL, LPS, PolyI:C, TNF-α, IL-1β, IFN-γ), each replicated three times. This was encapsulated within a colData DataFrame, which was paired with the gene_counts matrix to create a DESeqDataSet object. This object serves as the foundational data structure for subsequent DESeq2 operations. Pre-filtering: To enhance the efficiency and accuracy of our analysis, we filtered out genes with low read counts across all samples, retaining only those genes with more than 10 reads in total. This step reduces computational burden and improves the robustness of statistical inference. Normalization and Differential Expression Analysis: We executed the DESeq2 function, which internally performs several critical steps:

Size Factor Estimation: Adjusts for differences in library sizes across samples.Dispersion Estimation: Estimates gene-wise dispersion to account for biological variability.

Negative Binomial GLM Fitting and Wald Statistics: Fits a model for each gene and tests for differential expression.

Extracting Results: We generated results tables for specific comparisons (e.g., TNFa vs. CTRL), applying a $\log_2$ fold change threshold of 0 and an alpha of 0.05 to control the type I error rate.

Log_2 Fold Change Shrinkage: To improve the interpretability and stability of $\log_2$ fold changes, especially for genes with low counts or high dispersion, we applied the lfcShrink method using the 'ashr' approach. This method provides shrunken $\log_2$ fold changes, which are particularly useful for ranking and visualizing results.

Subset Significant Results: Post-analysis, we filtered the results to include only genes with adjusted p-values less than 0.05, focusing on those statistically significant changes in gene expression.

Following the differential gene expression analysis, we conducted a Gene Set Enrichment Analysis (GSEA) to identify significantly enriched gene sets that could elucidate the biological pathways involved in the response to different treatments. For this purpose, we utilized the clusterProfiler package, a powerful tool for comparing biological themes among gene clusters. The GSEA was performed using the gseGO function from the clusterProfiler package, which is specifically designed for Gene Ontology analyses. The parameters were set as follows:

geneList: This was derived from the DESeq2 results, where genes were ranked based on their $\log_2$ fold changes.

OrgDb: We used org.Hs.eg.db for *Homo sapiens* gene annotation.

keyType: Gene identifiers were specified as "ENSEMBL".

ont: We analyzed all categories of Gene Ontology: Biological Process, Cellular Component, and Molecular Function.

minGSSize and maxGSSize: The size of the gene sets considered for analysis was restricted to between 10 and 200 to ensure statistical robustness.

pvalueCutoff: A threshold of 0.05 was used to determine the significance of the enriched pathways.

verbose: Set to TRUE

seed: Set to TRUE

nPerm: We performed 10,000 permutations to assess the enrichment score, providing a robust estimate of the p-values.

eps: This parameter was set to 0.

In case of KEGG analysis we employed the gseKEGG function from the clusterProfiler package, which is tailored for KEGG pathway analyses. The parameters for the KEGG analysis were set similarly to those used in the Gene Ontology analysis with the following modifications:

organism: Set to "hsa" (*Homo sapiens*).

keyType: Set to "kegg" to utilize KEGG gene identifiers.

minGSSize: The minimum size of gene sets considered was adjusted to 5 to include more specific and potentially relevant pathways.

Subsequent to these analyses, we specifically focused on pathways related to DNA repair and DNA damage. Both the gseGO and gseKEGG analyses were refined to filter for gene sets associated with these pathways.

To address the issue of multiple comparisons and control the false discovery rate, the Benjamini-Hochberg (BH) method was employed for p-value adjustment in both analyses. This method systematically reduces the risk of type I errors, ensuring that the reported findings are statistically robust and less likely to result from random chance.

2.6. Visualization of gene expression

For the visualization of the different gene expression, we used the EnhancedVolcano and ComplexHeatmap packages, the exact version numbers are listed in the Key Resources Table.

To visualize the network connections of repair pathways, we used GOxploreR, ggraph, scatterpie and igraph packages.

The general workflow is illustrated in Fig. 1, and the tools used for the data analysis are presented in the Supplementary Materials.

2.7. Immunostaining of ADMSC cells

The samples were fixed for 20 min using 4 % paraformaldehyde and then washed three times with Phosphate Buffered Saline (PBS) solution. Subsequently, the tissues were permeabilized with 0.3 % Triton-X-100/PBS for 20 min at 25 °C. Then, sections were blocked with 5 % Bovine serum albumin/PBS (BSA/PBS) for 1 h. Samples were incubated with the following primary antibodies diluted in 1 % BSA/PBS with 0.1 % Tween 20 (1 % BSA/PBST): anti- γH2AX (Abcam ab26350) in 1:500, anti-53BP1 (Abcam ab36823) in 1:500. After washing steps, the following secondary antibodies were used: goat anti-rabbit IgG (H&L) Alexa 555 (Invitrogen, A21429) in 1:1000 and goat anti-mouse IgG (H&L) Alexa 488 (Molecular Probes, A11029) in 1:1000 dilution. Finally, cells were mounted with DAPI (4′,6-diamidino-2-phenylindole)-containing ProLong Gold antifade reagent (Life technologies). Samples were visualized with Olympus

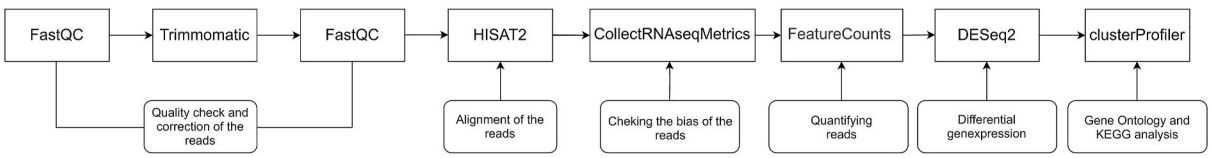

Fig. 1. The schematic representation of the bioinformatic pipeline for next-generation sequencing data processing.

FluoView FV10i confocal microscopy. The same exposition time was used for every image captured. Images were quantified with ImageJ software.

2.8. Image analysis of the confocal pictures

For the ImageJ analysis, we carefully chose ten cells from five distinct areas within each tissue section. During the analysis, in MatLab FoCo, the foci number was recorded and added to the database. FoCo is a graphical user interface created in Matlab's graphical user interface design environment. The computed values were displayed using box plots in Sigma Plot 12.0, and the significance of each sample was determined using independent samples t-tests in IBM SPSS Statistics 27.0.

2.9. qPCR analysis

RT-qPCR reactions were conducted in a final volume of 10 μL using the GoTaq qPCR Master Mix from Promega (Madison, WI, USA) on a QIAGEN Rotor-GeneQ 5-plex HRM qPCR System (Qiagen, Hilden, Germany). All RT-qPCR amplifications followed the same thermal cycling conditions: an initial denaturation at 95 °C for 7 min, followed by 40 cycles of 95 °C for 15 s and 60 °C for 560 s, and concluded with a melting curve analysis. Primers were designed using Primer3 software (https://primer3.ut.ee/) and are listed in Table 1. The specificity of the primers was verified using NCBI BLAST (http://www.ncbi.nlm.nih.gov/tools/primer-blast/). Each RT-qPCR measurement was performed in 2 technical duplicates.

The following primers were designed to evaluate the expression of the specific genes.

3. Results

To reveal the gene expression responses in the cells prepared for MSC transdifferentiation and transplantation, the following treatments were applied: (I) IL-1β to suppress inflammation in adipose tissue, (II) TNF-α to promote cell proliferation and differentiation while suppressing apoptosis, (III) PolyI:C used for priming or boosting therapy to unleash lymphocytes and other factors of the targeted therapeutic pathway, (IV) LPS to boost the immune plasticity of the cells, and (V) IFN-γ to improve therapeutic effectiveness. Cells were harvested, and RNA sequencing was performed on each group following each treatment, involving independent biological triplicates. After analyzing the datasets, principal component analysis (PCA) was conducted, which confirmed that each treatment brought on equivalent changes in the triplicates and produced unique gene expression profiles (Figs. 1 and 2A).

First, samples could be discriminated against depending on the treatment using PCA clusterization of the NGS data. The PCA plot also revealed that clusters involving the following specimens localize in close proximity: (I) LPS- and IL-1β-treated and (II) PolyI:C- and TNF-α-treated (Fig. 2A and B). Second, we examined the clusters based on differentially expressed genes compared to control. This analysis showed that control samples (referred to as CTRL in Fig. 2) can be sorted into the same cluster, similar to each treatment group. After successfully clustering the samples, we identified the differentially expressed genes affected by the applied treatments. In the case of TNF-α and PolyI:C, out of the 2755 and 2861 differentially expressed genes, 1533 and 1511 were upregulated, and 1222 and 1350 genes were downregulated, respectively. Upon IFN-γ, IL-1β, and LPS treatment, 2334 (1430 upregulated and 904 downregulated), 993 (380 downregulated and 613 upregulated), and 1614 (781 upregulated and 833 downregulated) differentially expressed genes were identified, respectively. The number of genes also exhibits a similar tendency to the results demonstrated by the PCA plot: those treatments, such as IL-1β and LPS, which are closer to the control cluster affect the gene expression of fewer genes. In contrast, PolyI:C, TNF-α, and IFN-γ treatments induce more robust gene expressional changes.

Furthermore, we conducted volcano plots to examine how the treatments influenced vital cellular pathways (Fig. 2C). The volcano plots indicate that DNA repair genes are predominantly upregulated in the treated MSC cells. The following numbers of genes associated with DNA repair were identified upon the treatments as follows: (I) TNF-α treatment—of 1533 upregulated and 1222 downregulated genes, 137 and 18 DNA repair-related genes, respectively; (II) LPS treatment—of the 781 upregulated and 833 downregulated genes, 107 and 7 DNA repair-related genes, respectively; (III) IL-1β treatment—of 613 upregulated and 380

Table 1
Sequences of the gene-specific primers used in qRT-PCR reactions.

Gene	Forward	Reverse
BRCA1	CTGAGGACAAAGCAGCGGAT	TCTTGATCTCCCACACTGCAA
CDC45	CAGCTCGGACAGGAAGAACTTT	ACAGGAGGGAAATAAGTGCGT
CDK1	GGGTCAGCTCGTTACTCAAC	CCCAAAGCTCTGAAAATCCTG
EXO1	ACACTAAGCTACGCTGGGC	TTCTTGAATGGGCAGGCATAG
FOXM1	TGGAGCAGCGACAGGTTAAG	TTGTGGCGGATGGAGTTCTTC
GTSE1	CTGCGGAGAAGCCCAAGAA	TTCCTTGCGAGATTGCTGGT
H2A.X	GTGCTGGAGTACCTCACCG	TGGCGCTGGTCTTCTTGG
HMGA2	GAAGACCCAAAGGCAGCAA	TTCAGTTTCCTCCTGAGCAG
MCM8	AGTCTTCCCACAAAGTGTCCT	TCCGACCTGCTTCTCTCTGAT
PLK1	AAGTACGGCCTTGGGTATCAG	GCAAGTGCTCGCTCATGTAA
POLQ	GCACACTGCTACAGGACGAA	TGCAGCTCTCTCCTCCATCT
UHRF1	ATGAGACGGAATTGGGGCTG	TTCTCCGGGTAGTCGTCGTA
XRCC2	CCGCGTCAATGGAGGAGAAA	TCCACATCACACAGTCGTCG

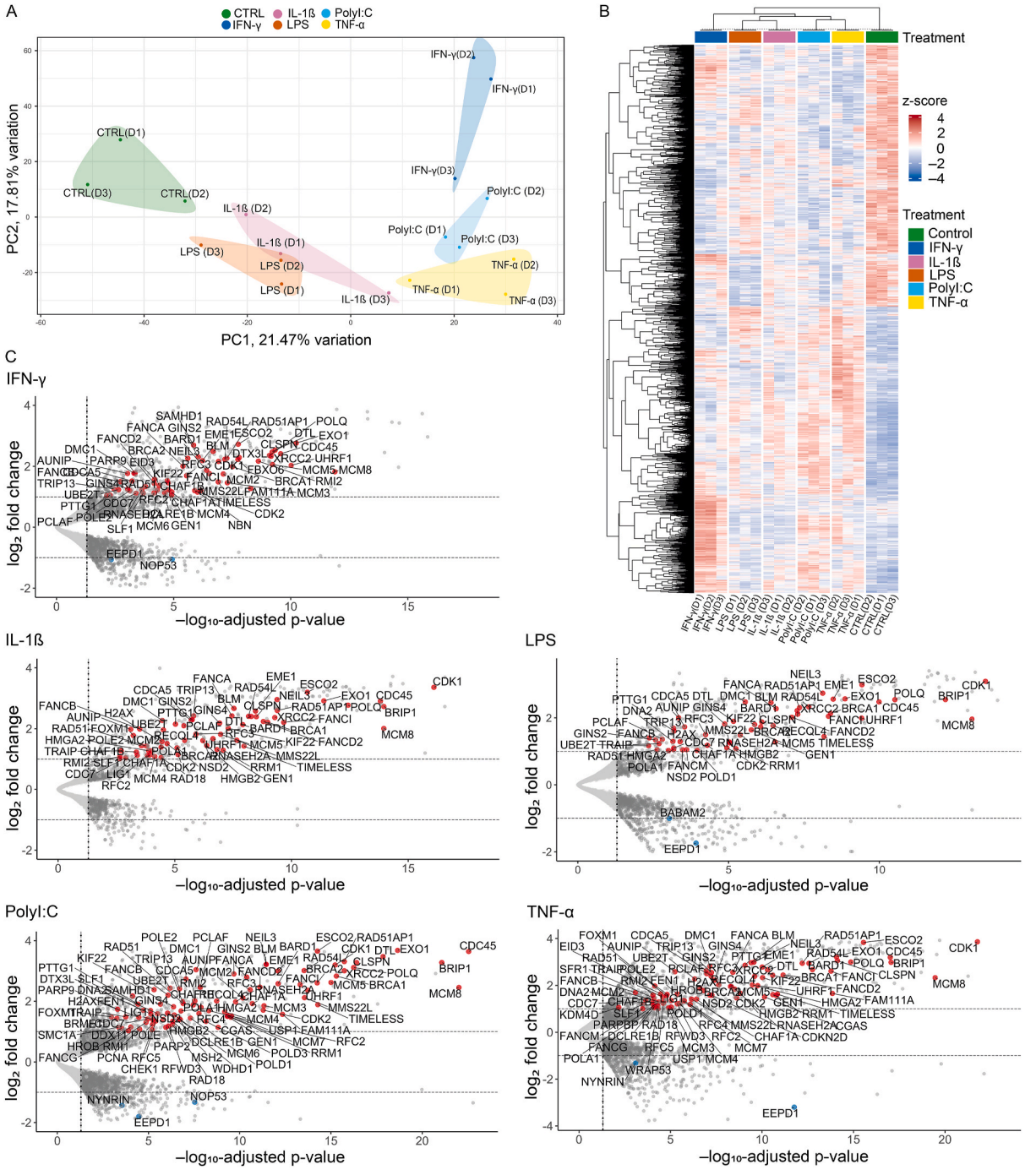

Fig. 2. Gene expressional changes in the stromal vascular fraction of human MSC cells following tumor necrosis factor (TNF-α), lipopolysaccharide (LPS), interleukin 1 beta (IL-1β), polyinosinic acid (PolyI:C), or interferon-gamma (IFN-γ) treatment. A) Principal component analysis of the dataset, B) Heatmap and cluster analysis of the differentially expressed genes. Red represents the upregulated genes with higher z-score, while blue indicates the downregulated genes. D1, D2, and D3 refer to the biological replicates. C) Volcano plot representation of the differentially expressed DNA repair-related genes. For visualization of the most significant DNA repair genes, we employed a cut-off value of 1 for absolute $\log_2$ fold-change (upper horizontal dashed line) and 0.05 for statistical significance (lower horizontal dashed line). The dotted vertical line denotes to $-\log_{10}$ ($P_{\text{cut-off}}$).

downregulated genes, 102 and 6 DNA repair-related genes, respectively; (IV) PolyI:C treatment—of 1511 upregulated and 1350 downregulated genes, 161 and 24 DNA repair-related genes, respectively; and (V) IFN-γ treatment—of 1430 upregulated and 904 downregulated genes, 131 and 16 DNA repair-related genes, respectively (supplementary files: 2, 3, 4, 5, 6). These results indicate that

each treatment induces intensive regulation in DNA repair pathways, and DNA repair-related genes are predominantly upregulated (Fig. 2C).

Pathway enrichment analysis revealed that all treatments brought on the upregulation of genes that encode proteins involved in the DNA double-strand break repair pathway (DSBR). PolyI:C treatment notably exhibited a more pronounced influence on DNA repair pathways than other treatments (Fig. 3A and B). PolyI:C induces reactive oxygen species (ROS) and activates etinoic acid-inducible gene I (RIG-I)-like receptors, affecting DNA repair pathways through RIG-I and ROS-mediated mechanisms, which may have an impact on the non-homologous end-joining pathway (Fig. 3A and B). TNF-α treatment demonstrated a broader effect on upregulating common DNA repair pathways in MSC cells. Aside from DNA repair pathways, TNF-α treatment can trigger various signaling pathways involving caspase, nuclear factor kappa B, p53, and c-Jun N-terminal kinase [17]. Intriguingly, negative regulation of DDR was also detected, indicating the multifaceted effects of TNF-α treatment (Fig. 3A and B). LPS, IL-1β, and IFN-γ treatments have fewer but common effects on DSBR pathways; however, IFN-γ exhibits the most negligible impact on the repair pathways (Fig. 3A and B). Network analysis visualized in a pie chart represents the connection between the treatments, the distribution of the treatments and the regulation of Gene Ontology (GO) terms. These results underlie that genes induced by PolyI:C treatment are implied in more DNA repair pathways than genes induced by the other treatments (Fig. 3C). To validate the results of the NGS analysis, 13 genes were selected from the list of DNA repair-related genes. We then quantified RNA expression levels across samples using qPCR, calculated the mean expression values, and depicted these average expression levels (Fig. 3D). The results show an upregulation of these genes, consistent with previous findings. Furthermore, to validate our *in silico* findings, we performed immunostaining on control and TNF-α-, LPS-, IL-1β-, PolyI:C-, or IFN-γ-treated MSC cells. We utilized an antibody against γH2AX, one of the initial DDR factors, to monitor if DNA repair is activated in treated cells. We observed significantly elevated levels of γH2AX following each treatment, indicating that MSC cells indeed activate the DDR pathway. Samples subjected to LPS treatment showed noticeably higher γH2AX levels (Fig. 4).

To further validate that the treatments affected DSBR, we employed an antibody specific to 53BP1 (Fig. 4). We also detected a significantly higher number of 53BP1 foci in TNF-α-, LPS-, IL-1β -, PolyI:C-, or IFN-γ- treated cells, respectively, which is consistent with the results of γH2AX. The highest value was observed in samples treated with LPS (Fig. 4). These data underscore that transcriptional reprogramming triggered by TNF-α, IL-1β, PolyI:C, IFN-γ, or LPS leads to DNA damage induction and initiates DSBR in adipose tissues.

4. Discussion

DNA repair is crucial for the physiological function of the cells, particularly in stem cells that differentiate into various cell types. Because of its protracted duplicative character, the bone marrow MSC population, constituting a small percentage (0.001 %–0.01 %) of cells, is susceptible to DNA damage [18]. This vulnerability arises from the accumulation of DNA errors in each progeny cell during replication. DNA damage in MSCs can be caused by various factors, including external physical and chemical agents, reactive oxygen species generated during inflammation, altered metabolic pathways, deamination, and hydrolysis. Because these activities can break DNA double helix or function as mutagenic sources, they can interfere with DNA transcription or replication [11,19]. The cell type, the duration and timing of the exposure to external and internal stimuli, and the cellular microenvironment affect how the cell reacts to these impacts. Although several mechanisms exist to correct DNA errors in early-passaging (young) MSC cultures *in vitro*, long-term culture and aging likely alter this dynamic *in vivo* [11,18,20–23].

Persisting DNA damage can induce downstream processes such as aging or cellular senescence. Genetic, epigenetic, transcriptional, and metabolic alterations, accompanied by decreased proliferation rate, are the hallmarks of aging. Several factors can cause DNA damage which accumulates in cells over time. The outcome depends on the balance between the extent of DNA damage and the capacity of the DNA repair system [22,24]. Excessive damage may overwhelm the repair mechanisms, leading to impaired biological functions such as loss of differentiation and regenerative capacity, cell death, mutagenesis, altered cell cycle and division, or senescence [11,18,25].

Senescence is a common phenomenon in aging or stressed MSCs [22,24]. Senescent MSCs undergo cell cycle arrest even though they are metabolically active. Senescence has a complicated molecular background that has dual effects. During tissue and organ formation, senescence inhibits cell division, yet it also protects against tumorigenesis by removing cells from the replicative cycle. Senescence elicits cell cycle arrest and is characterized by the emergence of a long-lasting cellular program known as the senescence-associated secretory phenotype (SASP). In this condition, senescent cells secrete numerous pro-inflammatory molecules into the tissue milieu, including IL-1, IL-6, IL-8, GROα/β, GM-CSF, MMP-1, MMP-3, MMP-10, ICAM-1, PAI-1, and IGFBPs [26–28]. Human mesenchymal stem cells that have been exposed to actinomycin D-induced senescence exhibit inhibition of DNA synthesis, reduction in the protein level of P21 and P16, elevation of β-galactosidase activity associated with senescence, and enlargement of γH2AX foci [29]. The SASP phenotype enhances the motility of lung tumor and osteosarcoma cell lines *in vitro*. While senescence benefits the preservation of the stem cell supply, the altered tumor microenvironment due to SASP may be detrimental to the organism [30]. Similar SASP appears in long-term cultures of senescent MSCs with different origins and certain hematological malignancies [24,26,31,32]. In addition to causing inflammation, the SASP phenotype attracts immune cells, which exacerbates microenvironmental inflammation [31]. Aging MSCs can induce neighboring cell aging *in vitro*, leading to a cascade effect [33]. The involvement of MSCs in tumor formation or metastasis remains controversial. Tumor suppressor mechanisms may be activated in response to the accumulation of DNA damage in MSCs, counteracting the resulting mutational burden. Various contexts highlight the complex interplay among senescence, MSC differentiation, and DNA repair. In certain cell types, DNA repair mechanisms are associated with epithelial–mesenchymal transition and metastasis, inhibiting differentiation [34–39]. In tumor cells, DNA repair-induced senescence is linked to increased pro-inflammatory molecule release, such as IL-6 and IL-8, which promote regeneration and migration processes

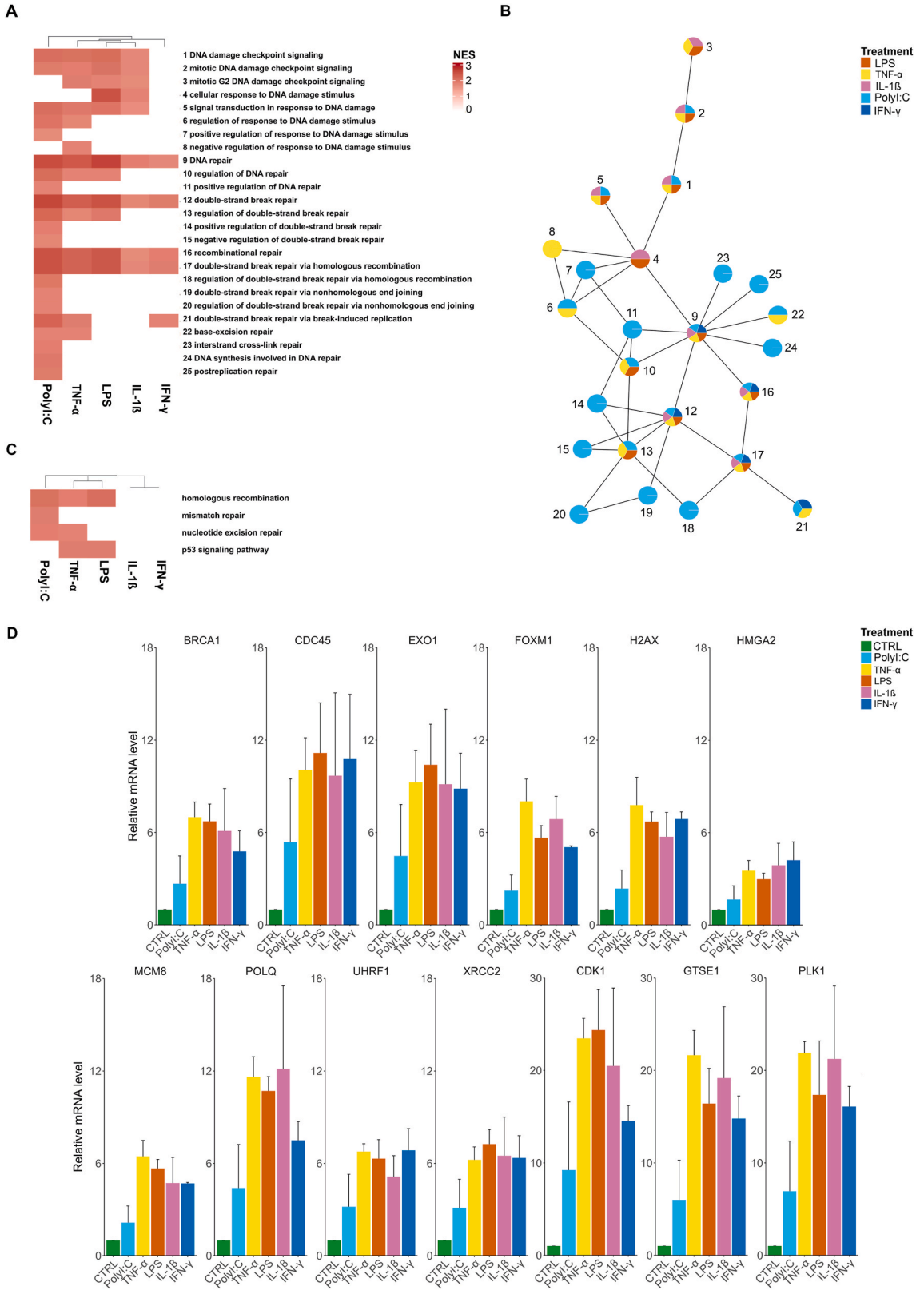

(caption on next page)

Fig. 3. The affected signaling pathways related to DNA repair in response to TNF-α, LPS, IL-1β, PolyI:C, or IFN-γ treatment. A) Schematic representation of the enriched DNA repair pathways in response to TNF-α, LPS, IL-1β, PolyI:C, or IFN-γ treatment. B) Dendrogram of the affected DNA repair pathways highlighted on panel A) where the network diagram indicates the proportions of treatments concerning various pathways. C) Enriched DNA repair-related pathways according to the KEGG database. D) The qPCR validation of the RNA-seq data the measured expression of each condition of the 13 genes are shown. The error bars represent the standard deviation.

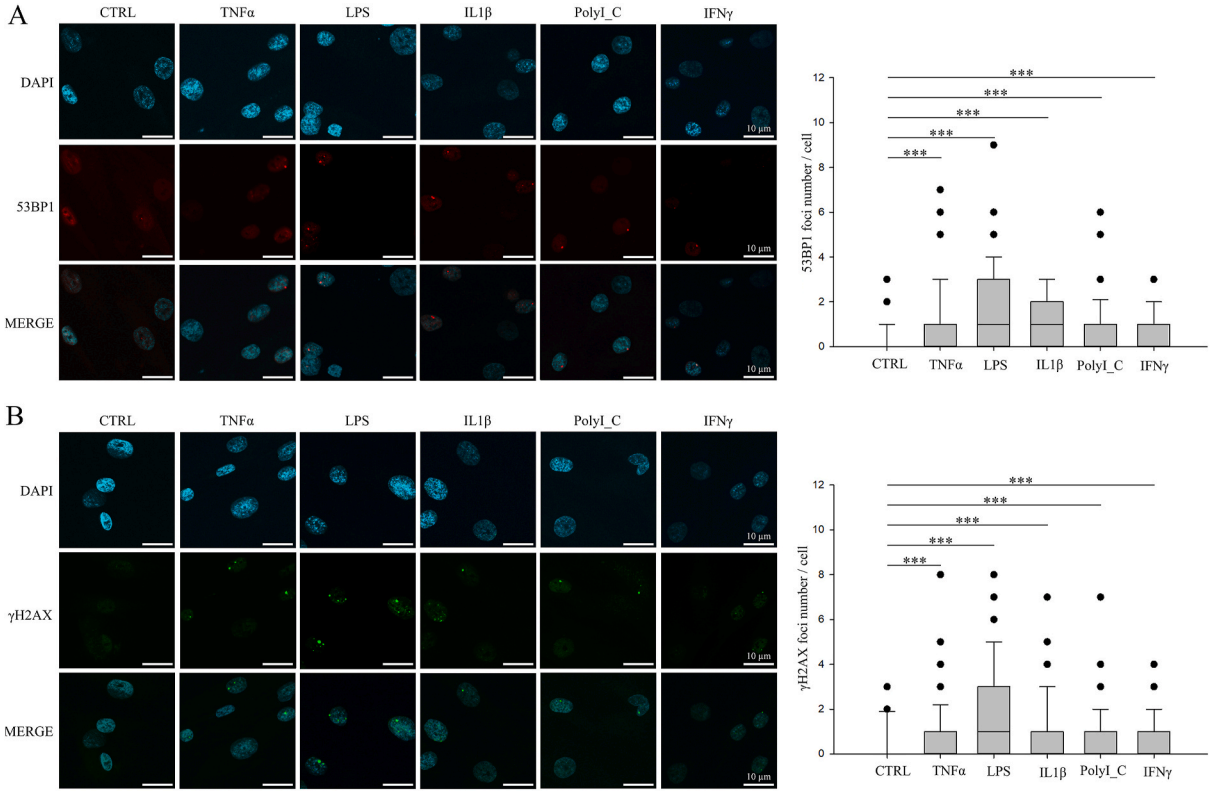

Fig. 4. Monitoring the changes of γH2AX and 53PB1 protein levels in ADMSC cells following TNF-α, LPS, IL-1β, PolyI:C, and IFN-γ. Confocal microscopy images of patient-derived cells treated with TNF-α, LPS, IL-1β, PolyI:C, or IFN-γ and stained with A) anti-53BP1 and B) γH2AX antibody. The quantification of the foci is depicted on the right side of each panel. The values represent the mean ± standard deviation from three independent experiments ($N = 100$ cells in each experiment). Statistical significance in both bar charts was calculated using independent samples t-tests ($P < 0.001$***).

[28]. Repairing DNA defects in MSCs is crucial as these defects act as trigger points for the differentiation of different types of cells and tissues. The impact of DNA damage on MSC differentiation is controversial. While some cases indicate that DNA damage can be beneficial and protective, according to others, it hinders the differentiation pathways [40,41]. The immunological status of the environment and the balance between cell division and differentiation are critical for maintaining tissue integrity. The role of MSCs in inflammation is multifaceted. MSCs can exhibit either immunosuppressive or inflammation-stimulating behaviors in an inflammatory environment, depending on the molecular background of inflammatory signaling. In this study, we discovered that MSCs responded to the inflammatory environment by increasing proliferative activity rather than undergoing senescence, even though inflammation, especially when associated with ROS production, can lead to senescence. Human umbilical vein endothelial cells (HUVECs) underwent senescence due to damage signal TNF-α, which resulted in persistent DNA damage via the inflammatory associated JAK/STAT pathways [17,42]. Additionally, it is known that TNF-α treatment increased the level of 8-Oxoguanine DNA glycosylase 1, indicating extensive DNA repair. PolyI:C is known to elicit inflammatory stimuli via the toll-like receptor 3 (TLR3) pathway and initiate more likely apoptotic outcomes instead of senescence [43]. Since viral infection may pose a threat to stem cells, elevated DNA repair may be indicated by the activation of the TLR3 pathway. In a subset of stem cells, repeated activation of the toll-like receptor 4 (TLR4) pathway by LPS increased the level of γH2AX and brought on senescence [44]. MSCs activated by TLR3 and TLR4 play a crucial role in tryptophan breakdown and kynurenine production, essential for effectively inhibiting T-cell proliferation. IFN-γ participates in multiple immune responses mediated by MSCs. IFN-γ treatment generates an immunosuppressive type of MSC which suppresses T-cell proliferation to induce either local or systemic immunosuppression; nonetheless, in certain cell types, IFN-γ can cause DNA damage [45].

The differentiation capacity and the unique immunosuppressive behaviour make MSC optimal candidates for therapeutic agents.

Sounak and colleagues have shown in a plant model that stem cells migrating to the wound play a chimeric role in wound healing. Successful migration to the distal wound site requires active DNA repair pathways, and continuous DNA repair mechanisms are required to maintain migration and wound healing. Currently, there are only a limited number of human studies on how DNA repair mechanisms can affect stem cell function. Most of the data are based on experience with bone marrow MSC *in vitro* culture, with a focus on how long-term culture affects genotoxicity and differentiation [46,47]. This is important in cell therapy procedures where pre-culture of cells is required. However, in most MSC-based procedures, there is no culture period, and cells are administered to patients immediately after isolation. In MSC-based procedures used in regenerative medicine, cells are placed in an inflamed, possibly infected environment, and little is known about their behavior *in vivo*.

In the case of hematopoietic stem cells, we know that deficiencies in repairing genotoxic damage may be responsible for the development of acute high-grade graft-versus-host disease (GVHD), increasing its risk [48,49]. More recently, iPS cells have become a focus of research, where it is even more important to preserve DNA integrity because they can accumulate a number of mutations [50]. hESCs have shown that the XPC-HR23B complex may play a role in regulating the "stem cell state" in human hESCs, which means that it may also be important for therapeutic use [51].

Our study indicates that induced ADMSCs exhibit higher expression of several mRNAs. The common set of these transcripts includes mRNAs that encode proteins involved in DNA repair. The main cause of persistent DNA damage may be extensive transcriptional reprogramming, resulting in the transcriptional activation of this gene set associated with DNA repair [52,53]. Our findings imply that if these errors remain unrepaired, they may play a significant role in the failure of the MSC therapy and cause premature aging and senescence.

5. Conclusions

In conclusion, as revealed by the detection of increased DNA repair foci formation, our study highlighted that the transcriptional reprogramming induced by TNF-α, LPS, IL-1β, PolyI:C, and IFN-γ activates the downstream DNA repair cascade. This can have an impact on the regeneration of the tissue and its immunological status. Given that MSCs have a robust differentiation and migration capacity, DNA damage induced by various factors can lead to significant and prolonged changes, even in cells already in the process of differentiation. When these errors remain unrepaired or undergo improper repair, they may lead to cellular malformation and potentially initiate further tumor formation or abnormal tissue regeneration in the recipient's body. Based on these results, the therapeutic options must be carefully reconsidered.

Ethics approval and consent to participate

The collection of adipose tissue complied with the guidelines of the Declaration of Helsinki and was approved by the National Public Health and Medical Officer Service (NPHMOS) and the National Medical Research Council (16821-6/2017/EÜIG, STEM-01/2017, 6 September 2017) which follows the EU Member States' Directive 2004/23/EC on the practice of presumed written consent for tissue collection for University of Szeged.

Consent for publication

Not applicable.

Funding

This research was funded by the National Research, Development and Innovation Office grant GINOP_PLUSZ-2.1.1-21-2022-00043 (Z.V.) co-financed by the European Union and the European Regional Development Fund. Tibor Pankotai is supported by the National Research, Development and Innovation Office under NKFI-FK 132080 grant (T.P.), Zoltán Veréb under NKFIH PD 132570 grant (Z.V.). Zoltán Veréb is a recipient of the János Bolyai Research Scholarship of the Hungarian Academy of Sciences (BO/00190/20/5) (Z.V.). The project received funding from the EU's Horizon 2020 Research and Innovation Program with grant agreement No. 739593 (T.P.). Project no. TKP-2021-EGA-05 has been implemented with the support provided by the Ministry of Culture and Innovation of Hungary from the National Research, Development and Innovation Fund, financed under the TKP2021-EGA funding scheme (T.P.). Project no. 2022–2.1.1-NL-2022-00005 has been implemented with the support provided by the Ministry of Culture and Innovation of Hungary from the National Research, Development and Innovation Fund, financed under the 2022–2.1.1-NL funding scheme (T.P.). The funders had no role in the study design, data collection and analysis, decision to publish, or preparation of the manuscript. Funders have no conflict of interest. The project also received fund from Hungarian Academy of Sciences (POST-COVID2021-36).

Ethics statement

Not applicable.

Availability of data and materials

All data generated and analyzed during this study are included in this manuscript. The datasets used and/or analyzed during the

current study are available from the corresponding author on reasonable request.

CRediT authorship contribution statement

Zoltán G. Páhi: Writing – original draft, Formal analysis, Data curation. **Diána Szűcs:** Supervision, Formal analysis, Conceptualization. **Vanda Miklós:** Visualization, Investigation. **Nóra Ördög:** Investigation. **Tamás Monostori:** Investigation. **János Varga:** Investigation. **Lajos Kemény:** Validation, Formal analysis. **Zoltán Veréb:** Visualization, Validation, Supervision, Resources, Project administration. **Tibor Pankotai:** Writing – review & editing, Writing – original draft, Visualization, Data curation.

Declaration of competing interest

The authors declare that they have no known competing financial interests or personal relationships that could have appeared to influence the work reported in this paper.

Acknowledgements

We are grateful to Dr. Barbara N. Borsos for her critical review and suggestions. We also grateful to Manuéla Katona for her contribution in qPCR quantification experiment.

Appendix A. Supplementary data

Supplementary data to this article can be found online at https://doi.org/10.1016/j.heliyon.2024.e36275.

References

[1] T. Reya, et al., Stem cells, cancer, and cancer stem cells, Nature 414 (6859) (2001) 105–111.
[2] A. Sada, T. Tumbar, New insights into mechanisms of stem cell daughter fate determination in regenerative tissues, Int Rev Cell Mol Biol 300 (2013) 1–50.
[3] P.C. Baer, Adipose-derived mesenchymal stromal/stem cells: an update on their phenotype in vivo and in vitro, World J Stem Cells 6 (3) (2014) 256–265.
[4] N. Song, M. Scholtemeijer, K. Shah, Mesenchymal stem cell immunomodulation: mechanisms and therapeutic potential, Trends Pharmacol. Sci. 41 (9) (2020) 653–664.
[5] C. Young, et al., A porcine model for adipose tissue-derived endothelial cell transplantation, Cell Transplant. 1 (4) (1992) 293–298.
[6] W.J. Jurgens, et al., Effect of tissue-harvesting site on yield of stem cells derived from adipose tissue: implications for cell-based therapies, Cell Tissue Res. 332 (3) (2008) 415–426.
[7] V. Roukos, T. Misteli, The biogenesis of chromosome translocations, Nat. Cell Biol. 16 (4) (2014) 293–300.
[8] A. Ciccia, S.J. Elledge, The DNA damage response: making it safe to play with knives, Mol Cell 40 (2) (2010) 179–204.
[9] S. Burma, et al., ATM phosphorylates histone H2AX in response to DNA double-strand breaks, J. Biol. Chem. 276 (45) (2001) 42462–42467.
[10] G. Mannino, et al., Adult stem cell niches for tissue homeostasis, J. Cell. Physiol. 237 (1) (2022) 239–257.
[11] B. Banimohamad-Shotorbani, et al., DNA damage repair response in mesenchymal stromal cells: from cellular senescence and aging to apoptosis and differentiation ability, Ageing Res. Rev. 62 (2020) 101125.
[12] D. Szucs, et al., Effect of inflammatory microenvironment on the regenerative capacity of adipose-derived mesenchymal stem cells, Cells 12 (15) (2023).
[13] D. Szucs, et al., Licensing effects of inflammatory factors and TLR ligands on the regenerative capacity of adipose-derived mesenchymal stem cells, Front. Cell Dev. Biol. 12 (2024) 1367242.
[14] M. Dominici, et al., Minimal criteria for defining multipotent mesenchymal stromal cells. The International Society for Cellular Therapy position statement, Cytotherapy 8 (4) (2006) 315–317.
[15] Z. Vereb, et al., Vessel wall-derived mesenchymal stromal cells share similar differentiation potential and immunomodulatory properties with bone marrow-derived stromal cells, Stem Cell. Int. 2020 (2020) 8847038.
[16] Z. Vereb, et al., Role of human corneal stroma-derived mesenchymal-like stem cells in corneal immunity and wound healing, Sci. Rep. 6 (2016) 26227.
[17] A.G. Alotaibi, J.V. Li, N.J. Gooderham, Tumour necrosis factor-alpha (TNF-alpha) enhances dietary carcinogen-induced DNA damage in colorectal cancer epithelial cells through activation of JNK signaling pathway, Toxicology 457 (2021) 152806.
[18] X. Bao, et al., Extended in vitro culture of primary human mesenchymal stem cells downregulates Brca1-related genes and impairs DNA double-strand break recognition, FEBS Open Bio 10 (7) (2020) 1238–1250.
[19] N. Chatterjee, G.C. Walker, Mechanisms of DNA damage, repair, and mutagenesis, Environ. Mol. Mutagen. 58 (5) (2017) 235–263.
[20] P.K. Wu, et al., Early passage mesenchymal stem cells display decreased radiosensitivity and increased DNA repair activity, Stem Cells Transl Med 6 (6) (2017) 1504–1514.
[21] P.B. Delben, et al., Human adipose-derived mesenchymal stromal cells from face and abdomen undergo replicative senescence and loss of genetic integrity after long-term culture, Exp. Cell Res. 406 (1) (2021) 112740.
[22] J. Liu, et al., Senescence in mesenchymal stem cells: functional alterations, molecular mechanisms, and rejuvenation strategies, Front. Cell Dev. Biol. 8 (2020) 258.
[23] M. Pustovalova, et al., Accumulation of spontaneous gammaH2AX foci in long-term cultured mesenchymal stromal cells, Aging (Albany NY) 8 (12) (2016) 3498–3506.
[24] J. Yu, et al., The replicative senescent mesenchymal stem/stromal cells defect in DNA damage response and anti-oxidative capacity, Int. J. Med. Sci. 15 (8) (2018) 771–781.
[25] M.H. Kim, et al., An in vitro culture platform to study the extracellular matrix remodeling potential of human mesenchymal stem cells, Acta Biomater. 170 (2023) 376–388.
[26] L.Y. Chou, C.T. Ho, S.C. Hung, Paracrine senescence of mesenchymal stromal cells involves inflammatory cytokines and the NF-kappaB pathway, Cells 11 (20) (2022).
[27] J.P. Coppe, et al., The senescence-associated secretory phenotype: the dark side of tumor suppression, Annu. Rev. Pathol. 5 (2010) 99–118.
[28] F. Rodier, et al., Persistent DNA damage signalling triggers senescence-associated inflammatory cytokine secretion, Nat. Cell Biol. 11 (8) (2009) 973–979.

[29] V. Minieri, et al., Persistent DNA damage-induced premature senescence alters the functional features of human bone marrow mesenchymal stem cells, J. Cell Mol. Med. 19 (4) (2015) 734–743.
[30] J. Morales-Valencia, et al., Therapy-induced senescence promotes breast cancer cells plasticity by inducing Lipocalin-2 expression, Oncogene 41 (38) (2022) 4361–4370.
[31] S.S. Lee, et al., Stress-induced senescence in mesenchymal stem cells: triggers, hallmarks, and current rejuvenation approaches, Eur. J. Cell Biol. 102 (2) (2023) 151331.
[32] N. Plakhova, et al., Mesenchymal stromal cell senescence in haematological malignancies, Cancer Metastasis Rev. 42 (1) (2023) 277–296.
[33] I. Vassilieva, et al., Paracrine senescence of human endometrial mesenchymal stem cells: a role for the insulin-like growth factor binding protein 3, Aging (Albany NY) 12 (2) (2020) 1987–2004.
[34] H.J. Lee, et al., The DNA damage transducer RNF8 facilitates cancer chemoresistance and progression through twist activation, Mol Cell 63 (6) (2016) 1021–1033.
[35] J. Wu, et al., Chfr and RNF8 synergistically regulate ATM activation, Nat. Struct. Mol. Biol. 18 (7) (2011) 761–768.
[36] H. Pu, et al., PARP-1 regulates epithelial-mesenchymal transition (EMT) in prostate tumorigenesis, Carcinogenesis 35 (11) (2014) 2592–2601.
[37] S. Woditschka, et al., DNA double-strand break repair genes and oxidative damage in brain metastasis of breast cancer, J. Natl. Cancer Inst. 106 (7) (2014).
[38] A.B. Sharabi, et al., Twist-2 controls myeloid lineage development and function, PLoS Biol. 6 (12) (2008) e316.
[39] D. Sosic, et al., Twist regulates cytokine gene expression through a negative feedback loop that represses NF-kappaB activity, Cell 112 (2) (2003) 169–180.
[40] M. Hu, et al., NAP1L2 drives mesenchymal stem cell senescence and suppresses osteogenic differentiation, Aging Cell 21 (2) (2022) e13551.
[41] P. Jiang, et al., Genetic modification of H2AX renders mesenchymal stromal cell-derived dopamine neurons more resistant to DNA damage and subsequent apoptosis, Cytotherapy 18 (12) (2016) 1483–1492.
[42] K. Fehsel, V. Kolb-Bachofen, H. Kolb, Analysis of TNF alpha-induced DNA strand breaks at the single cell level, Am. J. Pathol. 139 (2) (1991) 251–254.
[43] R. Kandhaya-Pillai, et al., TNFalpha-senescence initiates a STAT-dependent positive feedback loop, leading to a sustained interferon signature, DNA damage, and cytokine secretion, Aging (Albany NY) 9 (11) (2017) 2411–2435.
[44] X. Feng, et al., Repeated lipopolysaccharide stimulation promotes cellular senescence in human dental pulp stem cells (DPSCs), Cell Tissue Res. 356 (2) (2014) 369–380.
[45] Z.X. Yang, et al., IFN-gamma induces senescence-like characteristics in mouse bone marrow mesenchymal stem cells, Adv. Clin. Exp. Med. 26 (2) (2017) 201–206.
[46] I. Hare, et al., In vitro expansion of bone marrow derived mesenchymal stem cells alters DNA double strand break repair of etoposide induced DNA damage, Stem Cell. Int. 2016 (2016) 8270464.
[47] M. Kim, et al., Regulation of base excision repair during adipogenesis and osteogenesis of bone marrow-derived mesenchymal stem cells, Sci. Rep. 13 (1) (2023) 16384.
[48] M. Arora, et al., Polymorphisms in the base excision repair pathway and graft-versus-host disease, Leukemia 24 (8) (2010) 1470–1475.
[49] B. Thyagarajan, et al., Association between genetic variants in the base excision repair pathway and outcomes after hematopoietic cell transplantations, Biol. Blood Marrow Transplant. 16 (8) (2010) 1084–1089.
[50] P. Simara, et al., DNA double-strand breaks in human induced pluripotent stem cell reprogramming and long-term in vitro culturing, Stem Cell Res. Ther. 8 (1) (2017) 73.
[51] J.J. Ho, et al., Regulation of DNA demethylation by the XPC DNA repair complex in somatic and pluripotent stem cells, Genes Dev. 31 (8) (2017) 830–844.
[52] H. Shimada, et al., Senescence of chondrocytes in aging articular cartilage: GADD45beta mediates p21 expression in association with C/EBPbeta in senescence-accelerated mice, Pathol. Res. Pract. 207 (4) (2011) 225–231.
[53] M. Shimada, et al., Reprogramming and differentiation-dependent transcriptional alteration of DNA damage response and apoptosis genes in human induced pluripotent stem cells, J. Radiat. Res. 60 (6) (2019) 719–728.